Challenge Journal of Structural Mechanics

Energy & crack tip stress interactions in mixed mode I/III fracture of DX51 steel sheets

Claire De Marco Muscat-Fenech [a,*], Stephen Ciappara [b]

[a] *Department of Mechanical Engineering, University of Malta, Msida MSD2080, Malta*
[b] *London Offshore Consultants, Ibex House, 42-47 Minories, London EC3N 1DY, United Kingdom*

ABSTRACT

DX51D sheet is subjected to mixed mode I/III loading in a purposely designed fixture apparatus. The resulting stable crack-tip growth, direction, slant angle and typical factory-roof crack were observed and discussed as the loading mixity was varied. The total essential work of fracture or fracture toughness, for each mixity loading, was evaluated adopting energy methods during experimentation, whilst theory details how the total may be separated into its individual mode components. The fracture type and direction of crack path were based on the von Mises failure theory and the fracture criteria of maximum shear stress, maximum hoop stress and maximum normal stress along with the application of Hill's theory. The findings described clearly establish the link between the applications of the energy based equations governing crack initiation and propagation and the equations describing the stress field surrounding the crack tip in the mixed mode I/III field.

ARTICLE INFO

Article history:
Received 25 July 2016
Accepted 6 September 2016

Keywords:
Mixed mode
Failure criteria
Slant fracture
Fracture toughness
Stress intensity

1. Introduction

Structures constructed from ductile materials are often subjected to mixed mode loading conditions in tension (mode I), in-plane shear (mode II) and out-of-plane shear (mode III). Mixed mode I/III fracture in ductile thin sheets is quite involved resulting in a complex 3D stress and strain field around the crack tip.

Initial studies for mixed mode loading and the ensuing fracture failure criterion proposed by Erdogan and Sih (1963) suggested several criteria, the maximum hoop stress criterion (MHSC) - the crack propagates along the plane normal to the maximum hoop stress and that this maximum hoop critical stress is a material property and the maximum energy release rate (or Griffith theory) - the crack propagates in a direction perpendicular to the far field tensile load in a direction such that the crack maximizes its energy release rate and therefore independent of the load mode mixity. Investigators working with materials which fail in a brittle manner who compared such criteria are Suresh et al (1990), Macagno and Knott (1989), Royer (1988) and showed that the crack propagation direction and crack loads differ only slightly when applying the criteria to these brittle materials.

There has been much investigation undertaken on the individual mode and on mixed mode loading. The various criteria proposed by previous investigators are the maximum strain energy density, whereby the crack propagates along the plane with a minimum strain energy density criterion (Sih and Cha, 1974; Sih and Barthelemy, 1980; Chen et al., 1986); the maximum normal stress criterion MNSC, when the crack propagates along the plane normal to the maximum normal stress (Tian et al., 1928), (Yates and Miller, 1989); the maximun principal stress criterion - the crack propagates perpendicular to the maximun principal stress; the maximum strain energy release rate where the crack propagates along a direction which maximizes the energy release rate (Pook and Sharples, 1979; Pook, 1985; Chen et al.,1986; Yates and Miller, 1989). All these investigators note that the crack growth direction and the fracture loads differ only slightly no matter which criteria was applied.

* *Corresponding author*. Tel.: +356-2340-2106 ; Fax: +356-2134-3577 ; E-mail address: claire.demarco@um.edu.mt (C. De Marco Muscat-Fenech)
ISSN: 2149-8024 / DOI: http://dx.doi.org/10.20528/cjsmec.2016.09.019

Nomenclature

a	Crack length [m]
A	Surface area of the crack [m^2]
E	Young's modulus [N/m^2]
K	Stress Intensity Factor [Pa$\sqrt{m}$]
L	Crack length advance, leg length [m]
n	Work hardening exponent
R	Specific essential work of fracture [N/m]
r	Distance from crack tip [m]
t	Thickness [m]
u	Displacement [m]/Length [m]
U	Work done/Energy [J]
w	Width [m]
W	Work done [J]
W_f	Work of fracture [J]
W_b	Work of un/bending [J]
W_T	Work of twisting [J]
$x/y/z$	Coordinates
X	Load, force [N]
α	Direction of crack front [^{o}]
ε	Strain [/]
ϕ	Direction of relative motion [^{o}]
Λ	Elastic strain energy [J]
γ	Mode mixity loading angle for Mode I/III
τ	Shear stress [N/m^2]
θ	Direction of stress [^{o}]
Γ	Plastic strain energy [J]
ξ	Plastic level through sheet thickness [/]
ρ	Distance from crack tip through the thickness [m]
ρ	Radius of curvature [m]
σ	Stress [N/m^2]
σ_y	Yield stress [N/m^2]
σ_o	Strength coefficient [N/m^2]
I	Mode I component
III	Mode III component
I/III	Mixed-mode I/III component
b	Un/bending
c	Critical
t	Total
T	Twist
y	Yield
m/c	Machine
rel	Relative
CT	Compact tension
LEFM	Linear elastic fracture mechanics
MHSC	Maximum hoop stress criterion
MNSC	Maximum normal stress criterion
MSSC	Maximum shear stress criterion
SEN	Single edge notched

Various authors have also studied the mode I/III fracture in brittle materials and concluded that the tensile mode I dominated the Mode I/III loading and the resulting typical fracture surface is non-planar (Sommer, 1969; Knauss, 1970; Chai, 1988; Suresh and Tschegg, 1987; Suresh et al., 1990; Hsia et al., 1995, Chao and Liu, 1997). The fracture surface resulting from this mixed mode loading is quite irregular and the crack initiation angles are not easy to measure (Pook, 1985; Yates and Miller, 1989; and Lui et al., 2004). Crack propagation in ductile materials under mixed mode I/III loading results in a complex 3D stress and strain field, the resulting macroscopic fracture mechanism are highly dependent on the mixity ratio between mode I and mode III and the associated out-of-plane stress system. Work performed by Shah (1974), Williams and Ewing (1972), Feng et al. (1993), Hui and Zehinder (1993), Kamat and Hirth (1994), Kamat and Hirth (1996), Helm et al. (1997), Helm et al. (2001), Sutton et al. (2001) and Lan (2006) all show that the resulting fracture surface is heavily dependent on the material properties and mode mixity competition of mode I versus mode III. This is also to be shown in this investigation.

Transition fracture type in mixed mode I/III in ductile materials have been investigated by Erdogan and Sih (1963), Maccagno and Knott (1992), Chao and Liu (1997), Chao and Zhu (1999), Lui et al. (2004) using only linear elastic fracture mechanics (LEFM) to predict crack loading and crack path direction for both brittle and ductile materials using the material's strength ratio of shear stress to tensile stress, τ_c/σ_c, and that the material's failure is according to the classical Tresca and von Mises failure theories. This approach is also adopted in this investigation since complete solution for the elastic-elastoplastic-plastic case of mode I/III do not yet exist, although partial results have been provided by Pan and Shih (1992) which are at present not sufficient.

The specimen types for the out-of-plane mode I/III investigations have been varied. Sutton et al. (2001) and Lan (2006) use a single edge notch (SEN) plate for in-plane tension-torsion loading, whilst Wei et al (2005), Yan et al. (2007, 2009), Wei (2011), Li et al. (2011) use a CT SEN plate with a short initial starter crack length and analyse their results using FEA. A modification to the CT SEN is one with a longer starter crack, commonly called a two legged trouser tear specimen, which is to be used in this investigation. The longer legs SEN specimen geometry was initially used by Rivlin and Thomas (1953) and successive co-workers for the large deformation and non-linear elastic response of sheet rubber. Work on ductile thin sheet materials has been successful completed by Mai and Cotterell (1984) and Muscat-Fenech et al. (1992, 1992, 1994a, 1994b). The tests on the two leg specimens use the work energy method and determine the essential work of fracture.

The work described here is to combine the work/energy criterion of the essential work of fracture and the crack tip stress/stress intensity approach. Investigators tend to normally solve such mixed mode problems with either method independently. The primary scope of this work is to establish a link and show how, through successful experimental under takings, this connection can

be achieved, whilst introducing some novel approaches to the theoretical and experimental work. Mixed mode I/III testing in ductile sheet materials occur as a complicated affair, with many important fracture events taking place. The investigation is to break down the many aspects involved during this process and report the findings in a systematic approach. The governing equations of crack tip stresses together with traditional theories and fracture criterions predict the type, path direction and slant angle of the advancing crack. Ductile fracture theory, presented as a novel approach, will describe how the mode mixity loading conditions affect the resulting slant angle and fracture type. The work energy approach extends the application of the established two-legged trouser specimen to mixed mode loading and the determination of the essential work of fracture. In addition, a new method based on the geometrical and mode I/III loading conditions, can successfully partition the essential work of fracture into its pure mode values at each loading mixity angle. The testing regime presented here is the first of its kind.

2. Theory

2.1. Mode I/III analysis

The crack tip zone suffers the highest stress concentration for sheet material under mixed mode loading. Westergaard (1939), Irwin (1957), Sneddon (1946) and Williams (1957) were amongst the first to investigate and publish the solutions of the closed form expression for the crack tip stress, assuming anisotropic linear elastic material behaviour. The original Westergaard stress functions solved for limited crack problems and modification, Sih (1966), Eftis and Liebowitz (1972), Sanford (1979) to the theory gives greater applicability of the solutions. Mixed mode fracture problems are reported proposing the maximum hoop stress failure criterion, MHSC (Erdogan and Sih (1963) on brittle materials); the maximum shear stress criterion, MSSC (Maccagno and Knott (1992) on fracture of ductile materials); and the application of MHSC and MSSC to predict the fracture type transition (Chao and Liu, 1997; Chao and Zhu, 1999). Liu et al. (2004) and Chao and Zhu (1999) report that there is only a very small difference between the elastic and elastic-plastic crack tip solutions.

The current investigation describes and analyses the many aspects of this complex mode I/III fracture of thin sheet materials:

- the description of the initial crack tip stresses involved during the loading;
- the fracture type determined from the material's critical tensile and shear stress (applying the Tresca and von Mises failure theories for ductile materials) when compared to the mode I/III stress theoretical predictions, together with the fracture criterions of MSSC, MHSC and the maximum normal stress criterion, MNSC, when the crack propagates along the plane normal to the maximum normal stress;
- the path direction and slant angle of the propagating crack are also determined using the material stress intensity factors in the respective pure mode directions, K_I and K_{III};
- an energy criterion is applied to this analysis along with Hill's (1953) theory of ductile sheet materials;
- the mode I/III essential work of fracture for varying load mixity angle, γ is obtained through experiment;
- geometrical and energy considerations allow the total essential work of fracture, R to be separated into its individual (R_I and R_{III}) percentage contribution of each of the load mixity angle scenarios.

The approach considered here, linking the methods of traditional crack tip stresses and intensity factors to the essential work of fracture is an innovative approach for mode I/III testing.

2.2. Mode I/III crack tip stresses and fracture type determination

Following the same trend as other investigators, Erdogan and Sih (1963), Maccagno and Knott (1992), Chao and Liu (1997), Chao and Zhu (1999) and Liu et al. (2004) to the solution of problems involving mixed mode, the mixed mode I/II/III crack tip stress fields, using cylindrical (r, θ, z) coordinates are shown in Fig. 1.

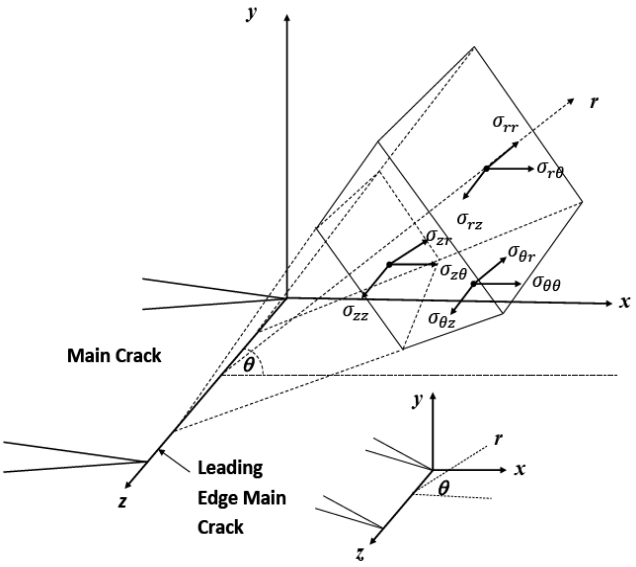

Fig. 1. Mixed mode I/II/III.

In thin ductile sheets, fracture is always a mixed mode affair, involving both the tensile effects (mode I) and out of plane shearing (mode III). To determine the fracture type, the maximum tensile, σ_{max} and shear stresses, τ_{max}, through the sheet thickness are required and compared to the material properties of critical tensile stress, σ_c and the critical stress in shear, τ_c. For tensile fracture; $\tau_{max}/\sigma_{max} < \tau_c/\sigma_c$ and for shear fracture: $\tau_{max}/\sigma_{max} > \tau_c/\sigma_c$ and applying the von Mises failure criteria for ductile materials in mixed mode loading, $\tau_c = 0.577\sigma_c$.

The tensile and shear stresses are obtained by a transformation through the thickness in the *yz*- plane is required. Such an element, through thickness plane, is shown in Fig. 2, the point is located at (ρ, α), where ρ is the distance of the element from the top face through the sheet thickness and α is the slant angle of the advancing crack plane. The slant angle is defined as the angle between propagating crack plane and the original flat crack plane. The slanting crack advance phenomena is observed and recorded in crack growth experiments in thin ductile materials, where the initially flat crack turns to a slant angle, α after a short flat-to-slant transition.

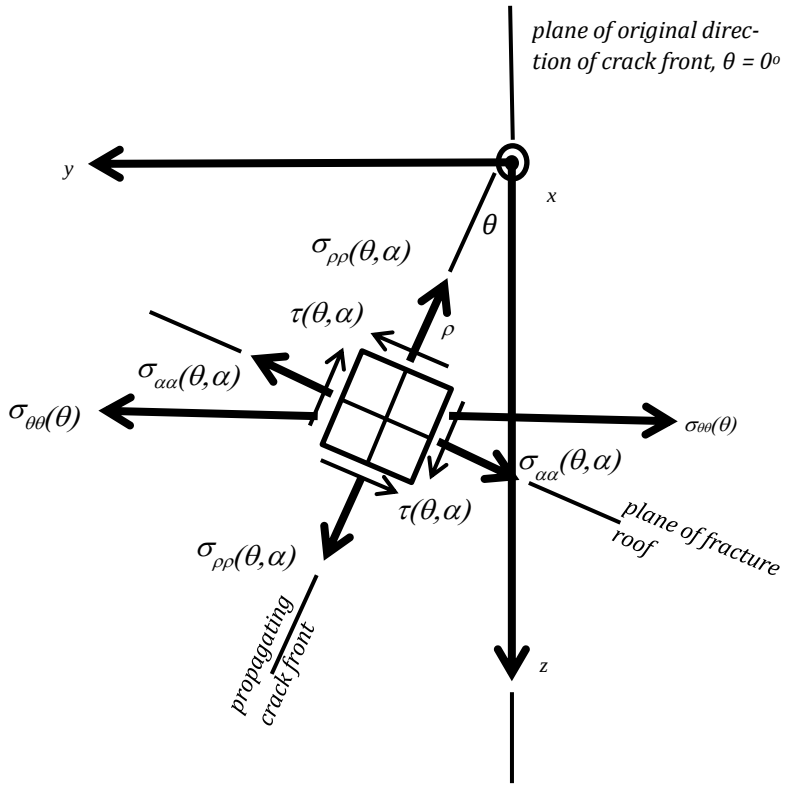

Fig. 2. Element at distance ρ in the *yz*- through thickness plane: Element (θ, α).

Chao and Zhu (1999) and Lui et al. (2004) give that for plane stress conditions, in the through thickness plane, under mode I/III, the crack tip tensile and shear stresses are:

$$\sigma(\theta,\alpha) = \frac{K_I}{\sqrt{2\pi r}} cos^3\frac{\theta}{2} cos^2\alpha - \frac{K_{III}}{\sqrt{2\pi r}} cos\frac{\theta}{2} sin\,2\alpha\,, \qquad (1)$$

$$\tau(\theta,\alpha) = \frac{K_I}{2\sqrt{2\pi r}} cos^3\frac{\theta}{2} sin\,2\alpha + \frac{K_{III}}{\sqrt{2\pi r}} cos\frac{\theta}{2} cos\,2\alpha\,. \qquad (2)$$

The above equations show that when a cracked body is loaded, it is possible that propagation is to occur either along a tensile fracture path at angle θ^* or along a shear facture path at an angle θ^{**} to the original direction of the crack front in the *xy*- plane. Whilst the plane of the crack front propagates inclined at an angle α ($\alpha^*$and α^{**}, tensile and shear respectively) in the through thickness *yz*- plane. In reality, the event is a combination of both individual fracture types, however the contribution of one mode over the other depends upon the mode mixity of loading. The contribution is discussed following the experimental investigation. From Lui et al. (2004) method for mode I/III, using the MNSC, MSSC and MNSC, the material (τ_c/σ_c) property and the stress intensity factors K_I and K_{III}:

$$\theta^* = 0^o \;\;,\;\; \alpha^* = \frac{1}{2} tan^{-1}\left[\frac{2}{-\frac{K_I}{K_{III}}}\right] \;\;,\;\; \frac{K_I}{K_{III}} = \frac{-2}{tan\,2\alpha}\,,$$

$$-\frac{\pi}{4} \le \alpha^* \le 0 \;\; for \;\; K_{III} \ge 0\,. \qquad (3)$$

In the plane of original direction of crack front, $\theta^* = 0^0$, Fig. 3 and slant angle, α^* the maximum tensile stress:

$$\sigma_{max} = \frac{K_I}{\sqrt{2\pi r}} cos^2\alpha^* - \frac{K_{III}}{\sqrt{2\pi r}} sin\,2\alpha^*\,. \qquad (4)$$

Introducing the critical stress intensity under mode I, $K_{IC} = \sigma_c\sqrt{2\pi r_c}$, where σ_c acts at critical distance from the crack tip r_c, the critical maximum tensile:

$$\frac{K_I}{K_{IC}} cos^2\alpha^* - \frac{K_{III}}{K_{IC}} sin\,2\alpha^* = 1\,. \qquad (5)$$

In Fig. 3, when $\alpha = \alpha^*$ the slant crack front is typically described as a factory roof appearance. $\sigma_{\alpha\alpha}$ is therefore parallel to the factory roof plane. In the case of $\sigma_{\alpha\alpha}(\theta^* = 0, \alpha^*)$, the fracture angle α^*, is also dependant on the loading/mixity angle γ This load mixity angle γ is to varied in this investigation between 0^o and 90^o, ($\gamma = 0^o$ - pure mode I; $\gamma = 90^o$ - pure mode III).

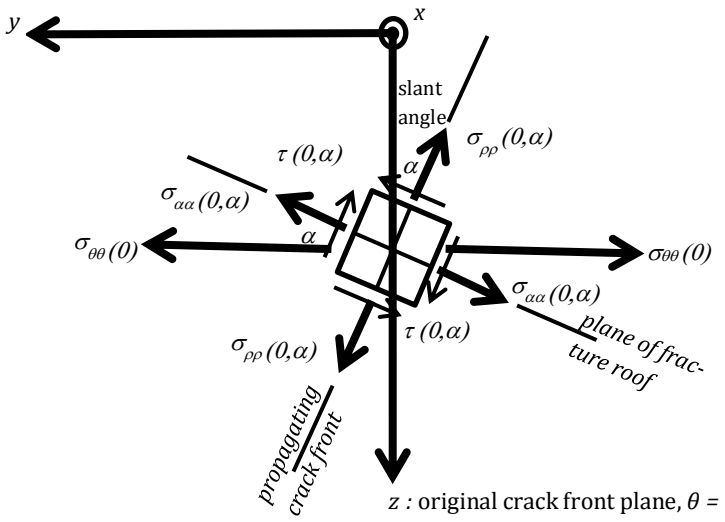

Fig. 3. Element at distance ρ in the *yz*- through thickness plane. Element $(\theta = 0^0, \alpha)$.

The maximum shear stress, along a plane at $\pi/4$ from that of the maximum normal stress, i.e. $\alpha^{**} - \alpha^{*} = \pi/4$, with α^{*} from Eq. (3) and $\theta^{**} = 0$, the slant angle and maximum shear stress are:

$$\alpha^{**} = \frac{1}{2} tan^{-1}\left[\frac{\frac{K_I}{K_{III}}}{2}\right], \tag{6}$$

$$\tau_{max} = \frac{K_I}{2\sqrt{2\pi r}} sin\, 2\alpha^{**} + \frac{K_{III}}{\sqrt{2\pi r}} cos\, 2\alpha^{**}\,. \tag{7}$$

In this condition, the crack roof is at an angle of $(\pi/2 + \alpha^{**})$ from the original crack plane, as shown in Fig. 3. If the maximum shear stress reaches the critical shear stress of the material, with $\tau_c = K_{IC}/\sigma_c\sqrt{2\pi r_c}$, then $(\sigma_c/\tau_c)\left((K_I/2K_{IC})\sin 2\alpha^{**} + (K_{III}/K_{IC})\cos 2\alpha^{**}\right) = 1$. Therefore, for the transition between the type of failure can be concluded according to the equations:

$$\frac{\tau}{\sigma} = \frac{\frac{1}{2}\left(\frac{K_I}{K_{III}}\right) sin\, 2\alpha^{**} + cos\, 2\alpha^{**}}{\left(\frac{K_I}{K_{III}}\right) cos^2\alpha^{*} - sin\, 2\alpha^{*}}, \tag{8}$$

$$\frac{K_I}{K_{III}} = \frac{cos\, 2\alpha^{**} + \frac{\tau}{\sigma}\, sin\, 2\alpha^{*}}{\frac{\tau}{\sigma}\, cos^2\, \alpha^{*} - \frac{1}{2} sin\, 2\alpha^{**}}. \tag{9}$$

2.3. Energy criterion

The work required to propagate a crack by unit area is defined by the essential work of fracture, also referred in literature as the fracture toughness, *R*. The essential work of fracture attains a critical value R_c when cracking initiates, whilst during quasi-static crack propagation, the material will crack at constant *R*.

For a material containing a starter crack of area *A*, the quasi-static incremental interchanges, as the body is loaded by an external force *X* and associated displacement *u*, produces a change in the elastic and plastic strain energy and the fracture work. The level of strain either surrounding the crack tip, or in the surrounding material dictate the strain energies involved.

The work equations are:

$$Xdu = d\Lambda + d\Gamma \quad \text{(before crack propagation) and} \tag{10}$$

$$Xdu = d\Lambda + d\Gamma + RdA$$
(during quasi-static crack propagation). (11)

The essential work of fracture, *R* is obtained from the experimental force-displacement *X*-*u* plots using the energy, *U*. From Eq. (11):

$$R = \left(\frac{\partial U}{\partial A}\right) x = -\left(\frac{\partial U}{\partial A}\right) u\,. \tag{12}$$

During mixed mode I/III loading, for each fixed loading mixity angle, the slant angle initially increases with crack extension, during the flat to slant transition. Eventually a steady state slant angle is achieved. The fracture surface is rough with the actual fracture area larger than the assumed planar surface. As a result of this increased surface, the material fracture process zone requires an increase of the work rate input to the system in the early stages. From the initial flat fracture surface, during the initial stages, the low toughness central region of the sheet material burrows through the material ahead of the surface. The burrowing produces the observed characteristic stretching on the outer surface. The surface is pulled along and propagation occurs under increasing load. The flat starter crack twists into the slant fracture. As a consequence the essential work of fracture also increases during this early transition stage producing the characteristic *R* – *A* crack growth resistance curves. For the thin sheet material tested here, the growth of the large crack tip zone is not completed before the crack starts to advance.

Results show that the *R* curve is characteristic of the material and independent of starting crack length, however dependent with rate, temperature and environment. In addition, it is found that the resistance to cracking, *R* and hence *K*, changes with thickness of the body.

The concept of K and hence R, changing with thickness with specimen thickness is all part of the same related process. Under plane stress conditions there is a low constraint to flow at the outside of the body due to the stress-free surfaces, however when plain strain conditions apply the interior material is not able to flow. Variations of essential work of fracture with material thickness are found in most materials.

2.4. Mode I/III specimen

Different specimens have been used for mixed mode I/III investigations. Sutton et al. (2001) and Lan (2006) use a single edge notch (SEN) plate for in-plane tension-torsion loading. Wei et al. (2005), Yan et al. (2007, 2009), Wei (2011), Li et al. (2011) use a CT SEN plate with a short initial starter crack for out-of-plane mode I/III testing. Zhu (2011) use an all fracture (AFM) rectangular bar SEN specimen.

The specimen chosen for this investigation is an SEN specimen with long initial starter crack length, also commonly called a two legged trouser tear specimen. The trouser tear test was initially used by Rivlin and Thomas (1953) and successive co-workers for the large deformation and non-linear elastic response of sheet rubber. This specimen has been adopted with success by many investigators for ductile sheet materials to determine the essential work of fracture R in pure mode III investigations (Mai and Cotterell, 1984; Muscat-Fenech et al., 1992; Muscat-Fenech and Atkins, 1994a, 1994b; Muscat-Fenech, 1992). Various material models have been used whilst, Muscat-Fenech (1992), Muscat-Fenech et al. (1992), Muscat-Fenech and Atkins (1994a) analyse the energy balance of tearing, mode III, in thin sheet materials made of elastoplastic material. This two legged trouser specimen has proved to provide valid and reliable test data. Muscat-Fenech (1992), Muscat-Fenech et al. (1992), Muscat-Fenech and Atkins (1994a, 1994b) have analysed the effect of the geometrical sizes of leg length, L, leg widths, w and material thickness, t on the ensuing crack path propagation. The leg length has to be sufficient to allow the material to bend and unbend freely as the crack path aligns itself for propagation. The legs widths must be equal, otherwise the crack path will diverge into the narrow leg with region, Muscat-Fenech and Atkins (1994a, 1994b).

For any material model characteristics, ranging from elastic to elastoplastic to rigid plastic, the work energy Eq. (11), as shown by the investigators who have successfully adopted this method as described above, always result in an equation of the form:

$$\frac{X}{t} = \frac{R}{2} + w \quad \{function\ of\ \sigma_y, \rho, E, t, \xi\}. \tag{13}$$

The variables in the { } brackets are geometrical and material properties. ρ is the radius of curvature of the leg width w, which is different in magnitude for each leg width, w of thickness, t and hence a function of the level of the plastic region ξ through the sheet thickness. The {function of $\sigma_y, \rho, E, t, \xi$} describes the strain energy per unit volume and encompasses and represents all the bending, unbending and twisting work interchanges experienced by the legs.

The above equation would at first glance indicate that a plot of force per unit thickness, (X/t) versus leg width, w gives a straight line with intercept $(R/2)$. However this is *not* the case. The straight line indicated in Eq. (13) is usually a best fit polynomial curve. The typical curve increases in value, maximises and then decreases as the leg width increases, (also present in this investigation). This occurrence is due to the competition and balance between the work of fracture W_f and the work of un/bending W_b and work of twisting W_T, Muscat-Fenech et al. (1992, 1994a). The work of un/bending and twisting are far from unimportant as often inferred by many investigators. In fact the specimens used by Wei et al. (2005), Yan et al. (2007, 2009), Wei (2011), Li et al. (2011) clearly shows the clamping region with sharp kinks at the edges of the clamps and the overall specimen deformation. The leg lengths are too short to allow the natural irreversible plastic deformation work to form completely and allow complete un/bending and un/twisting of the specimen. This surely had an effect on the crack tip stress and strain field, the angle of crack propagation and angle of the slant crack front.

2.5. Link between the energy and crack tip stress methods

The energy and crack tip stress (involving the stress intensity factors) methods both describe the same process. The essential work of fracture R, quantifies the net change in energy that accompanies an increment of crack extension; whilst the stress intensity factor K quantity characterizes the stresses, strains and displacements near the crack tip. The energy release rate describes global behaviour, whilst the stress intensity factor is a local parameter. As such K has nothing to do with fracture. However, for a specimen undergoing deformation the total strain energy stored per unit volume $= (1/2)\,\sigma\,\epsilon = (1/2)(\sigma^2/E)$ is obtained as the area under the force displacement, X-u plot. Griffith proposed that the elastic energy stored in the plate due to the presence of the crack to be: $U* = \sigma^2 \pi a^2\, t/E$ resulting that $\sigma = K/\left(Y\sqrt{\pi a}\right)$. In principle σ may be substituted in terms of K, such that $(1/2)(K^2/EY^2\pi a)$ and is integrated for the whole body. Therefore the R in quasi-static propagation must also be expressible in terms of K, hence the K of the propagating crack also serves to characterise a material's resistance to crack propagation and it may be an alternative parameter to R. The process zones contains the fracture events themselves and the K dominated characterisation of fracture can be successfully applied so long as the process zone is small around the crack tip. Atkins and Mai (1985), Anderson (2005), amongst many others, both report that from many experiments by other researchers, that test pieces using the same material give comparable constant K value during propagation as does R. Whilst many associate K to (σ, a) combinations at the start of cracking, this constant K that ensues with cracking is in fact like R. In fact, both the K and R values are often referred to as fracture toughness, explaining why in this work R is referred to as the essential work of fracture

and K as the stress intensity factor. The confusion between the two normally arises since the stress intensity factor $K = \sigma Y\sqrt{\pi a}$ is produced in a cracked body by the applied stress σ and the critical stress intensity factor K_c is of the material. When cracking occurs, the applied stress intensity factor reaches the critical value. K and R are related via Young's Modulus E, by the equation $K^2 = ER$. Equations involving the essential work of fracture R determine the loads and therefore the stress to cause fracture as does the above equation for $= \sigma Y\sqrt{\pi a}$, therefore a relation between the two must exist. Just as K refers to the mode of opening by the subscripts I, (II) and III, R is normally written as simple R without a subscript, here the notation to describe the mode of opening is to be extended and use the same notation of I, (II) and III to R.

2.6. Separation of the essential work of fracture mode I/III components

Hill (1953) originally suggested a yield criterion of ductile sheets in which the specimens form localised necks along the line which will develop into fracture. The mode I/III test specimens clearly show how the originally full thickness crack edge, not only turns and adjusts itself along the slant angle α, depending on the mode mixity γ, but also shows visible localised necking. The direction of slant angle α through the material thickness, is suggested here, to follow Hill's theory, such that: $\tan\alpha = (1/4)\cot\gamma$. The loading or mixity angle, γ is varied such that $\gamma = 0^0$ (mode I) and $\gamma = 90^0$ (mode III), to follow Hill's loading angle direction terminology. The relative motion as the crack proceeds with the mixity angle γ is illustrated in Fig. 4 and this approach allows the total essential work of fracture under mixed mode loading I/III to be split into its individual pure mode components.

The relationship of the direction of relative motion with ratio of strains is:

$$tan\,\alpha = \frac{u_{III}/u_{III_o}}{u_I/u_{I_o}} = \frac{\epsilon_{III}}{\epsilon_I}, \tag{14}$$

where u_I and u_{III} are the change in length, with respect to mode I and III, of the original gauge length u_{I_o} and u_{III_o} respectively, with the strains ϵ_I and ϵ_{III} parallel to the mode I and Mode III axes respectively as marked as gauge length points on the specimens..

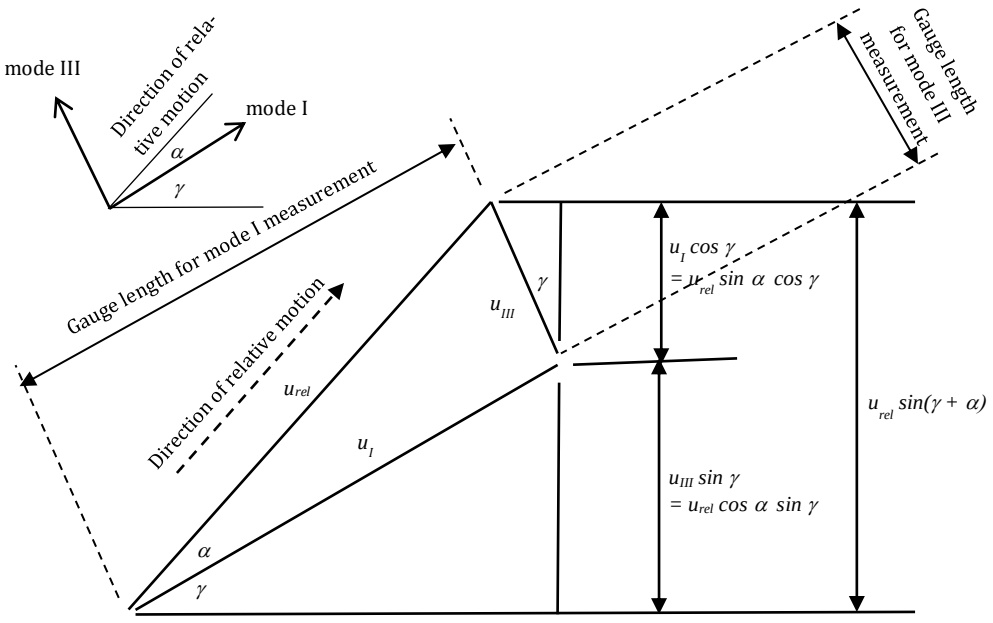

Fig. 4. Displacement components for mode I/III.

From the specimen geometry and displacements, the cross head, displacement $u_{m/c}$ can be defined as:

$$u_{m/c} = \epsilon_I u_{I_t} cos\,\gamma + \epsilon_{II} u_{IIIt}\, sin\,\gamma = u_{rel}\, sin\,\alpha\, cos\,\gamma + u_{rel}\, cos\,\alpha\ sin\,\gamma = u_{rel}\, sin(\gamma + \alpha)\,, \tag{15}$$

where u_{I_t} and u_{III_t} are instantaneous measured total length between the gauge indicators in the respective directions.

Moreover in a ductile body (such as steel), the deformation occurs in the direction at which the body is being loaded, therefore, considering the deformation into each mode, such that, $u_I = f(R_I)$ and $u_{III} = f(R_{III})$, then:

$$\frac{u_I}{u_{III}} = f(\,tan\,\gamma)\,, \tag{16}$$

$$\frac{u_{III}}{u_I} = g\left(\frac{R_{III}}{R_I}\right) = h(cot\,\gamma, tan\,\alpha)\,. \tag{17}$$

Since the total energy contribution during loading is:

$$U_T = \int_0^{u_{m/c}} X\ du = X u_{rel}\, sin(\gamma + \alpha)\,, \tag{18}$$

The total energy U_T is split into the two modes I and mode III, U_I and U_{III}, as follows:

$$U_I = \int_0^{u_I} X\ du = X u_{rel}\ sin\alpha\ cos\gamma\ ,$$

$$U_{III} = \int_0^{u_{III}} X\ du = X u_{rel}\ sin\gamma\ cos\alpha\ . \quad (19)$$

From Eq. (12), the total essential work of fracture, R and the components in the I and III direction are:

$$R = -\frac{\partial(U_t)_u}{\partial A} = \frac{X}{Lt} u_{rel}\ sin(\gamma+\alpha)\ , \quad (20)$$

$$R_I = -\frac{\partial(U_I)_u}{\partial A} = \frac{X}{Lt} u_{rel}\ sin\alpha\ cos\gamma\ ,$$

$$R_{III} = -\frac{\partial(U_{III})_u}{\partial A} = \frac{X}{Lt} u_{rel}\ cos\alpha\ sin\gamma\ . \quad (21)$$

The percentage contributions of each mode essential work of fracture, $\%R_I$ and $\%R_{III}$, to the total R with the varying loading mixity angle, 0^0(mode I) $< \gamma <$ 90^o(mode III), is expressed as:

$$\%R_I = \frac{R_I}{R} = \frac{sin\alpha\ cos\gamma}{sin(\gamma+\alpha)}\ ,$$

$$\%R_{III} = \frac{R_{III}}{R} = \frac{sin\gamma\ cos\alpha}{sin(\gamma+\alpha)}\ . \quad (22)$$

Hence, for quasi-static cracking in plane stress conditions, applying the standard relationship, $K^2 = ER$, together with Hill's yield criterion and ratio R_{III}/R_I gives:

$$\frac{R_{III}}{R_I} = \frac{\frac{X}{Lt}u_{rel}\ cos\alpha\ sin\gamma}{\frac{X}{Lt}u_{rel}\ sin\alpha\ cos\gamma} = \frac{cos\alpha\ sin\gamma}{sin\alpha\ cos\gamma} = \frac{tan\gamma}{tan\alpha} = 4\ tan^2\gamma =$$

$$\left(\frac{K_{III}}{K_I}\right)^2 R = -\frac{\partial(U_t)_u}{\partial A} = \frac{X}{Lt} u_{rel}\ sin(\gamma+\alpha)\ , \quad (23)$$

Substituting Eq. (24) into mode I/III Eq. (9) in terms of τ/σ , $\alpha^*$and α^{**}, then:

$$\frac{R_I}{R_{III}} = \left[\frac{cos\ 2\alpha^{**}+\frac{\tau}{\sigma}\ sin\ 2\alpha^*}{\frac{\tau}{\sigma}\ cos^2\alpha^*-\frac{1}{2}sin\ 2\alpha^{**}}\right]^2\ , \quad (24)$$

3. Experiments: Material, Specimen and Fixtures

The mixed mode I/III specimens are manufactured from galvanised low carbon steel, grade: DX51D. The mechanical properties of the material, in orientations of 0^0, 45^0 and 90^0 to the cold roll direction, are shown in Table 1, were determined in accordance with BS EN ISO 6892-1, 2009. (Instron 4206 tensile testing machine, crosshead machine speed of 1.8mm/min according to range 2.)

Table 1. Material Properties for DX51D.

Angle to rolling direction, ^{0}	0	45	90	Average
Young's Modulus, *E*, GPa	198	203	197	198
Ultimate Tensile Strength, MPa	355	354	357	355
Lower Yield Strength, MPa	313	305	297	305
Upper Yield Strength, MPa	321	324	303	318
Strain Hardening Exponent, *n*	0.279	0.323	0.291	0.304
Strength Coefficient σ_o, MPa	670	701	683	689

Mixed-mode I/III testing was performed on two legged specimens, Fig. 5. The material is of thickness, *t* of 0.6 mm and 1mm and leg widths, *w* of 12 mm, 24 mm, 36 mm and 48 mm, the total overall specimen length of 150 mm, allows a 12 mm clamping length, with starter crack lengths, *a* of 100 mm. The length of the leg or starter crack length *a*, was decided upon after several specimens were bent to ensure that the length of the leg is adequate for a natural curvature to form and prevent kinking in the clamped regions.

Specimens were clamped in the specially designed mixed-mode I/III jigs. The fixtures were designed to ensure no rotation of the fixture when coupled with the testing machine, such that in- and out-of-plane un/bending or twisting of the specimen is due to the test conditions. The specimens were loaded by the displacement controlled Instron 4206 tensile machine, with a crosshead machine speed of 8 mm/min. The load mixity angles chose are: $\gamma = 90^0$ (Pure Mode III), 67.5^0, 45^0 and 22.5^0. Pure mode I, $\gamma = 0^0$, testing conditions were not undertaken since proper pure mode I loading could not be established. However, the Mode I data $\gamma = 0^0$, was obtained from De Marco Muscat-Fenech and Ciappara (2013), since the same material was used in both investigations.

4. Experimental Results and Discussion

4.1. Essential work of fracture, R

Graphs of load-displacement were plotted for all the specimens obtained from data acquisition, with a sampling rate every 0.25s. Fig. 6, shows the force-displacement, *X-u* graphs, tests carried out at a loading mixity angle of $\gamma = 67.5^0$ and leg widths *w* = 12, 24, 36 and 48mm for specimens having a thickness of 1mm. The graphs illustrated in Fig. 6 being typical of the tests carried out in this investigation.

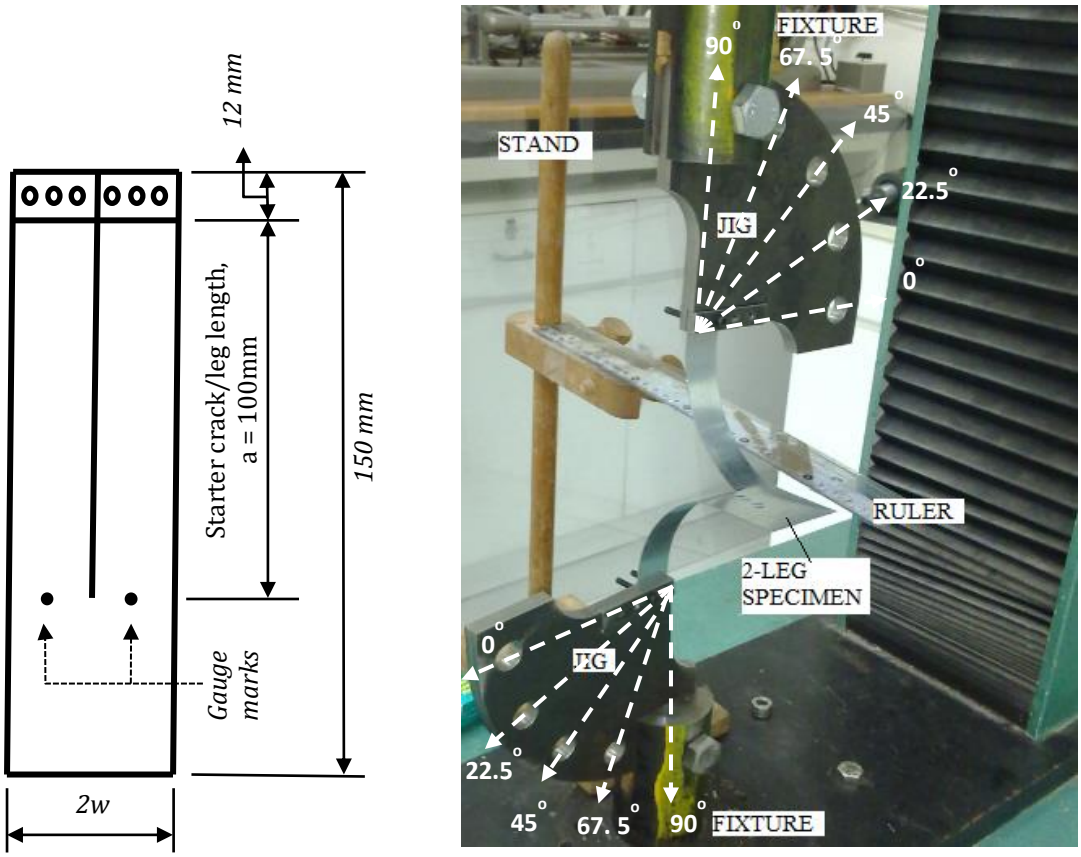

Fig. 5. Mode I/III specimen testing: (a) specimen; (b) testing $\gamma = 90^0$.

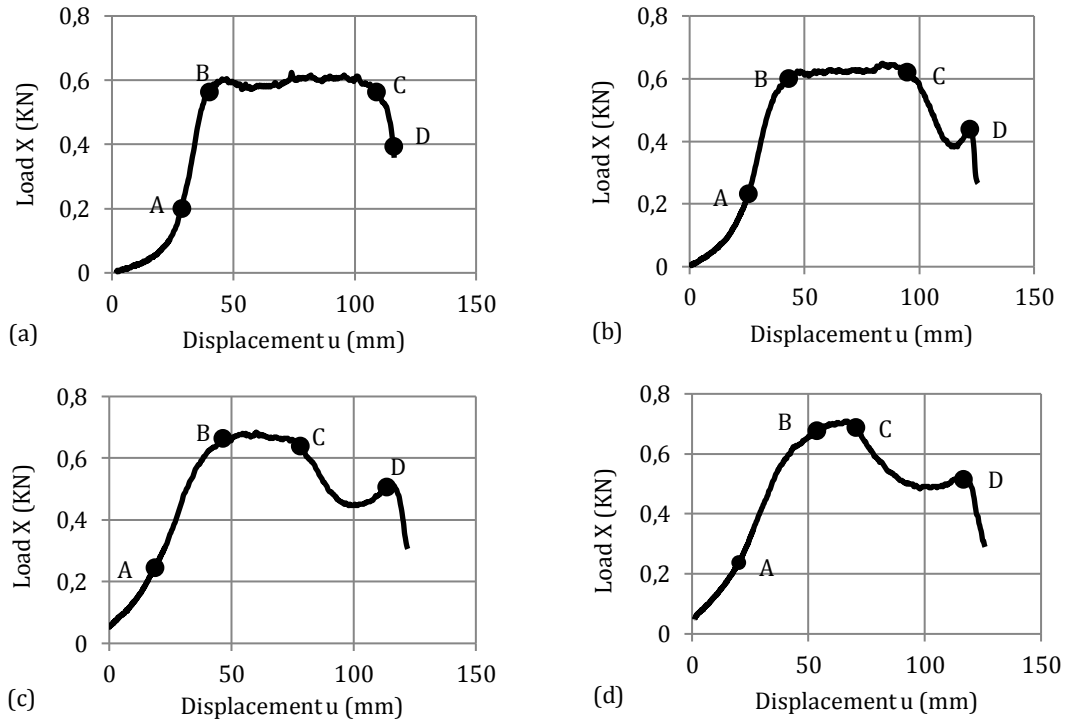

Fig. 6. Load-displacement graphs at loading angle $\eta = 67.5^0$, sheet thickness, t = 1mm, leg width: (a) w = 12mm; (b) w = 24mm; (c) w = 36mm; (d) w = 48mm.

A, B, C and *D*, are important points of interest for understanding the process during mixed-mode I/III testing, which will be used to extract useful information. From the origin *O* to point *A,* work is done to un/bend and twist the legs. Point *A* is the instant of visible tip deformation. Initially the magnification x50 of the camera was utilised to ascertain the onset of this deformation and a trained experimental eye for this instant was required. Point A marks the initial stage of the changes to occur ahead of the flat fracture surface. On the line between point A and B, the low toughness central region of the sheet material burrows through the material ahead of the surface, the crack tip is forming the characteristic triangular highly localised stretching region. During this time the crack tip front is orientating to establish its natural direction, the flat starter crack twists into the slant angle for the ensuing crack propagation. Growth of the large crack tip zone is not always complete before the crack starts to advance.

Point B marks the onset of crack propagation. Crack detection strain gauges placed as close as possible to the manufactured crack tip, but not in the triangular region detected the onset of the ensuing crack advance, in addition to visual observation of the onset of propagation. From point B up to C the crack propagates at constant load. This constant average force value is of particular interest in calculating the essential work of fracture, *R,* during stable crack propagation. Of noticeable interest is the fact that, as the leg width, *w* increases the constant force stable crack propagation magnitudes, first increases, maximises and subsequently starts to drop in value. This occurrence is very common and expected in two legged trouser tear tests. After point C, the load started to decrease, this results due to edge effects. The crack front is experiencing sizing and edge effects as in standard SIF test piece sizing problems. At point D, the load increased as the crack reached the edge of the specimen, when the specimen separated.

Applying Eqs. (12) or (13), the force per unit thickness, (X/t) for the varying widths, *w* for the different thickness, *t* and loading mixity angles γ, are plotted. First considering the values at the point, *A*, initiation of visible tip deformation; then for the constant crack propagation force values between the points *B* and *C* when stable and established crack propagation is occurring. The plots are shown in Figs. 7 and 8 respectively for both sheet thickness, *t* = 0.6 mm and 1.0 mm.

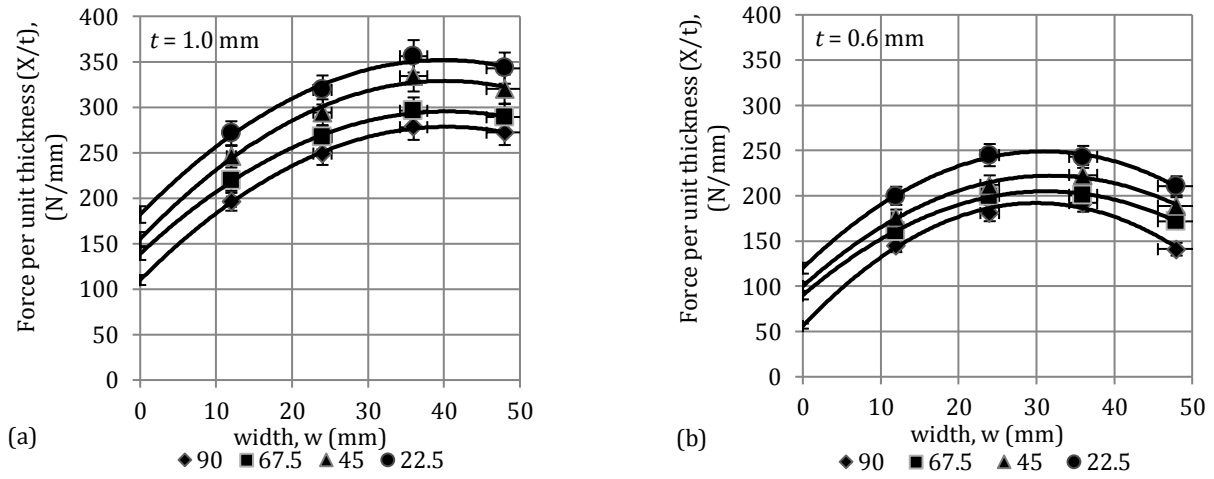

Fig. 7. Graphs of (load/thickness), (X/t), against width, *w*, at initiation point *A*, loading angles $\gamma = 90^0, 67.5^0, 45^0 and\ 22.5^0$. 5% error bars shown. Specimen sheet thickness: (a) *t* = 0.6 mm; (b) *t* = 1.0 mm.

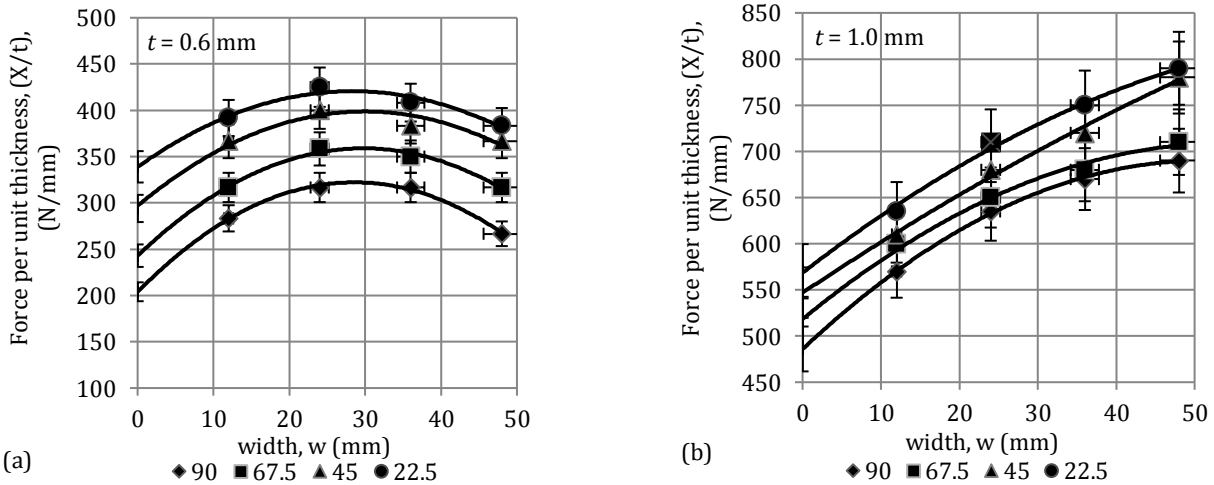

Fig. 8. Graphs of (load/thickness), (X/t), versus width, *w*, during crack propagation (*B* to *C*), loading angles γ = 90⁰, 67.5⁰, 45⁰ and 22.5⁰. 5% error bars shown. Specimen thickness: (a) *t* = 0.6 mm; (b) *t* = 1.0 mm.

From the plots of (X/t) versus w, as first observed by Muscat-Fenech (1992, 1994a) that such curves do not exhibit a linear behaviour as original intended by Mai and Cotterell (1984). Muscat-Fenech et al. (1992, 1994a) showed how the curvature of the leg ρ increases as the width w (and also the thickness, t) of the leg increases, the curvature is attributed to the varying amounts of the elastic and plastic work occurring during the process, i.e. the competition between the work of fracture W_f, the work of un/bending W_b and work of twisting W_T. In narrow leg widths of material of the same thickness, t, the work of fracture has the dominant effect of the system, whilst as the leg width increases, the work contributions to un/bending and twisting start to equal and then surpass the work of fracture. Consequently, also as the sheet thickness increases, the elastic work/energy plays a major role in the process which is readily noticeable when comparing the same material of various thicknesses, Figs. 7 and 8. The resulting curves are locus lines of the constant magnitudes of the essential work of fracture, R. The intercept on the (X/t) axis according to theory (Eq. (13) gives a value of $(R/2)$).

The values of essential work of fracture for crack initiation and propagation obtained from Figs. 7 and 8 are given for comparison in Table 2. As expected the variation of values of the essential work of fracture have occurred with the difference in material thickness. A common occurrence and is expected in ductile materials, as in the case that the stress intensity factor varies with thickness. R and K are closely related since the energy and crack tip methods both describe the same process.

4.2. Mixed mode components R_I and R_{III}

The procedure developed, taking into account the geometrical and testing conditions for the mode I/III investigated here, allows the total essential work of fracture under mixed mode loading I/III to be split into its individual pure mode components R_I and R_{III} for the various mixity angles, γ using Eqs. (22) and (23). The combined essential work of fracture and individual values at each mixity angle are given in Table 3 and plotted in Fig. 9.

Table 2. The essential work of fracture, R at initiation and crack initiation (Figs. 7 and 8 respectively, using Eq. (13)) for different loading angles and sheet thickness.

	$R_{\text{initiation}}$ (N/mm)		$R_{\text{crack propagation}}$ (N/mm)	
γ (deg)	t = 0.6 mm	t = 1 mm	t = 0.6 mm	t = 1 mm
90.0	112	220	408	972
67.5	180	278	486	1036
45.0	201	310	594	1094
22.5	242	364	678	1137

Table 3. Essential work of fracture $R_{I/III}$ and components R_I and R_{III}.

γ (deg)	90 (mode III)	67.5	45	22.5	0 (mode I)
			t = 0.6 mm		
$R_{I/III}$ (N/mm)	408	486	594	678	363
R_I (N/mm)	0	20	119	402	363
R_{III} (N/mm)	408	466	475	276	0
			t = 1 mm		
$R_{I/III}$ (N/mm)	972	1036	1094	1137	364
R_I (N/mm)	0	43	219	674	364
R_{III} (N/mm)	972	993	875	463	0

4.3. Validation of Hill's theory. Relation to the work/energy method and crack propagation direction

The findings below are to serve the following purposes. To investigate:
1. the validity of Hill's (1953) theory together with the relationship of the work/energy approach,
2. to compare the work/energy approach with the crack tip stress approach
3. the crack angles and direction

1. *Validity of Hill's theory and energy approach:* Using Hill's theory and the work energy method, the variation in the ratios R_I/R_{III} and therefore K_I/K_{III} can be investigated according to the loading/mixity angle γ, using Eq. (23), tabulated in Table 4 and plotted in Fig. 10.
2. *Crack tip stress approach:* Using the crack tip stress approach for values of the ratio and τ/σ, the K_I/K_{III} and R_I/R_{III} values can be plotted, applying Eqs. (9) and (24), Fig. 11.

Using the experimental values of the DX51D steel sheet tested under pure mode I and mode III, the average

ratio values of R_I/R_{III} and the corresponding values K_I/K_{III} are calculated. For the mode I/III theory based on the K_I/K_{III} value, the angles α^*, α^{**} and τ/σ can be evaluated, Table 5. For this low carbon steel material, DX51D, as investigated here, for the experimentally evaluated R_I/R_{III} ratio, the strength ratios predicted by the theory lie between $0.7 < \tau/\sigma < 0.77$; the τ/σ value range found is an acceptable for steel sheet.

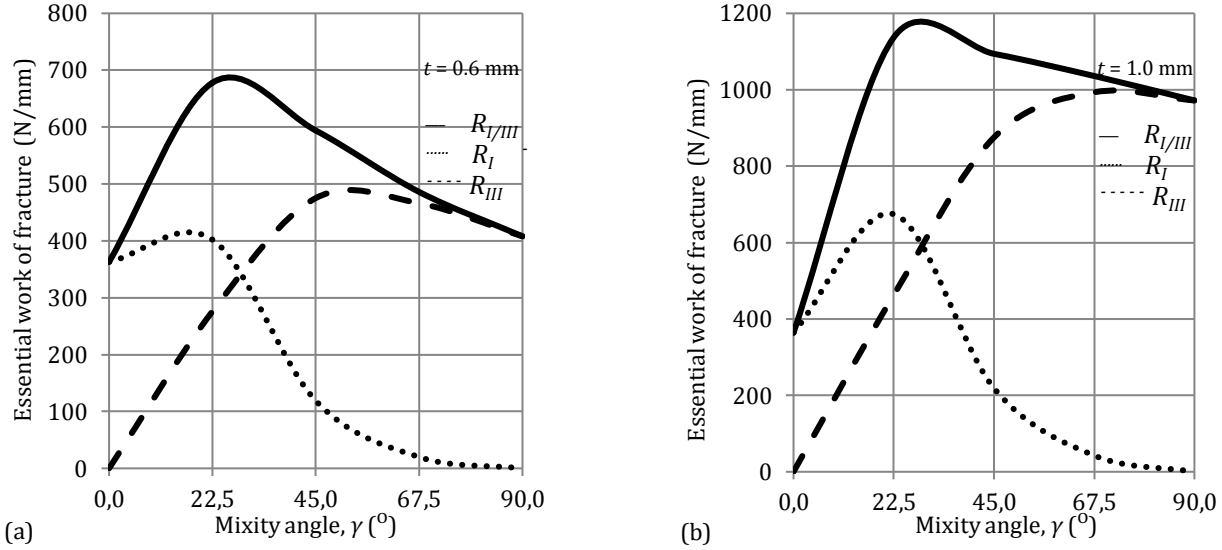

Fig. 9. Graphs of $R_{I/III}$, R_I and R_{III} versus the loading/mixity angle γ: (a) t = 0.6 mm; (b) t = 1.0 mm.

Table 4. R_I/R_{III} and K_I/K_{III} ratios for the variation in the loading/mixity angle γ.

γ (deg)	90 (mode III)	67.5	45	22.5	0 (mode I)
R_I/R_{III}	0	0.04	0.25	1.46	∞
K_I/K_{III}	0	0.2	0.5	1.2	∞

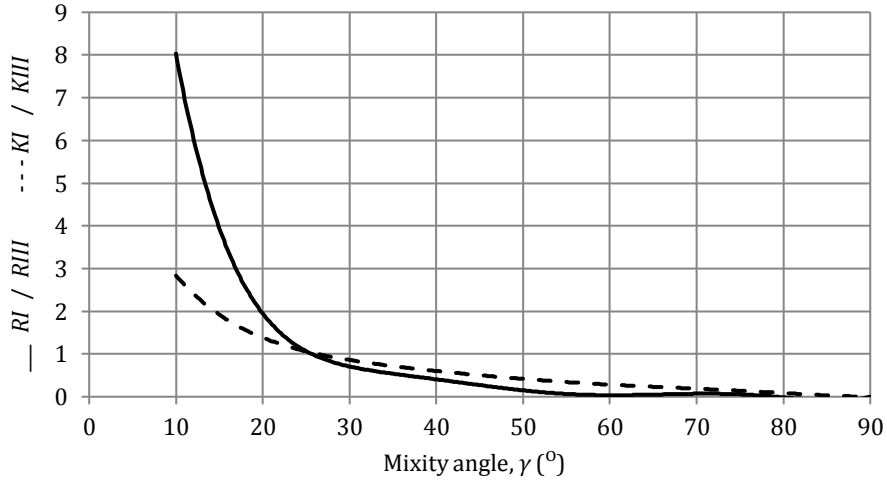

Fig. 10. Variation in ratios R_I/R_{III} and K_I/K_{III} with the loading/mixity angle γ.

3a. *Crack slant angles:* The crack tip stress theory predicts, applying Eqs. (3), (6) and (9), the angles α^* and α^{**} for the various τ/σ values. The relationship $K^2 = ER$, links the loading/mixity angle γ ((Eq. (23)) to the angles α^* and α^{**}. These theoretical relationships between all these variables and the experimental slant angle α (Table 6) are shown in Figs. 12 and 13, respectively. The experimental slant angle data clearly show very close proximity to the α^{**} shear failure curve. Fig. 14 shows the final link between the energy/work method to the crack tip stress approach, (applying together Hill's theory, the energy/work method and mode I/III theory presented here). Using the von-Mises, τ_c/σ_c=0.577 tensile to shear failure transition line, Fig. 14 shows that for the material tested the transition from tensile-to-shear failure occurs at: loading/mixity angle, $\gamma = 13.1^0$, $R_I/R_{III} = 4.62$, $K_I/K_{III} = 2.156$, $\alpha^* = -21.47$, $\alpha^{**} = 23.5^0$.

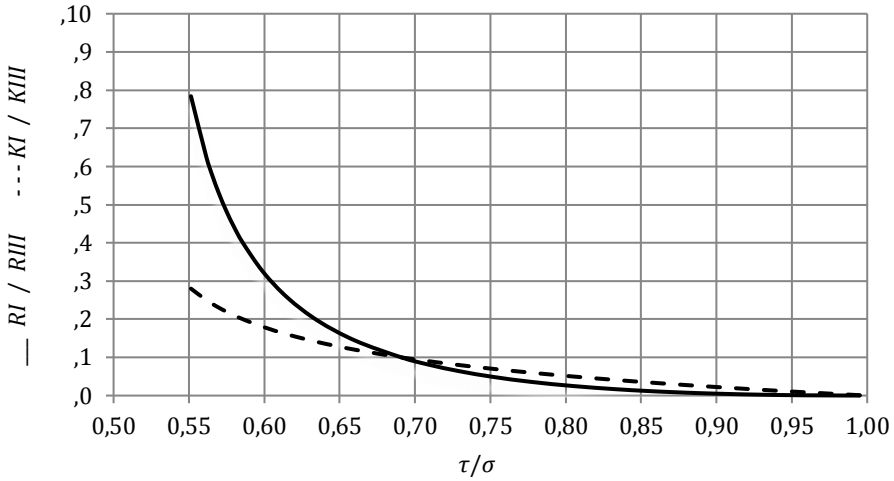

Fig. 11. Variation of τ/σ with K_I/K_{III} and R_I/R_{III} using the crack tip stress approach.

Table 5. DX51D sheet experimental/mode I/III theory evaluation.

Thickness t (mm)	0.6	1.0
R_I (N/mm)	363	364
R_{III} (N/mm)	408	972
R_I/R_{III}	0.89	0.37
K_I/K_{III}	0.94	0.61
α^* (deg)	32.4	36.5
α^{**} (deg)	12.6	8.4
τ/σ	0.70	0.77

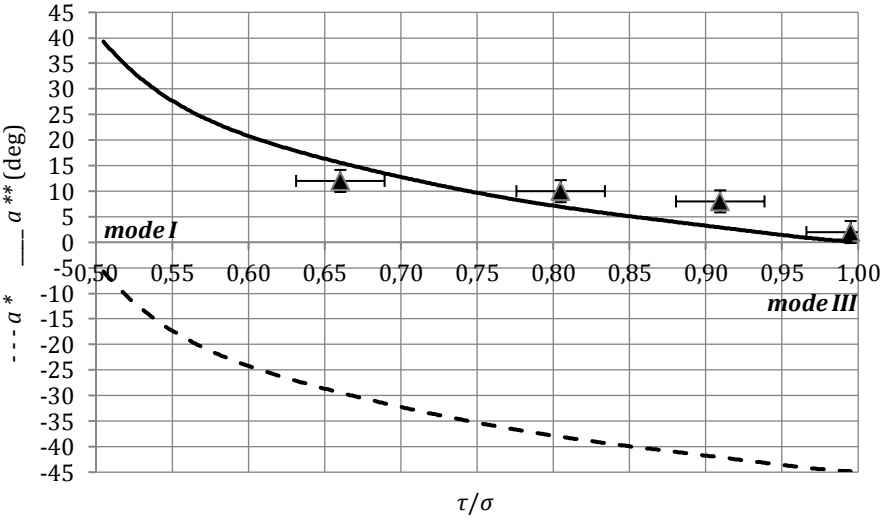

Fig. 12. Variation of α^* and α^{**} with τ/σ , ▲ experimental showing the standard error.

3b. *Crack path direction:* Every specimen, for each leg width w, thickness t and mixity angle γ, the value of the experimental direction angle of the crack path θ were obtained by measurement. The experimental direction angle of the crack path θ, for such tests is expected and also predicted by theory to be 0°. This crack path direction is also noted by Muscat-Fenech (1992), Muscat-Fenech and Atkins (1994a), who show that the direction of the crack path is simply a function of the relative widths of the leg widths w and any deviation is soley dependant on the relative leg widths. For equal widths the crack path is down the centre line. With slight variations of differences in the leg widths, the crack path diverges from the centre line kinking into the narrower width material section. During the experimental work the crack path deviation from the centre line was noted to be very minimal, only up to maximum angles of 3°, within experimental error.

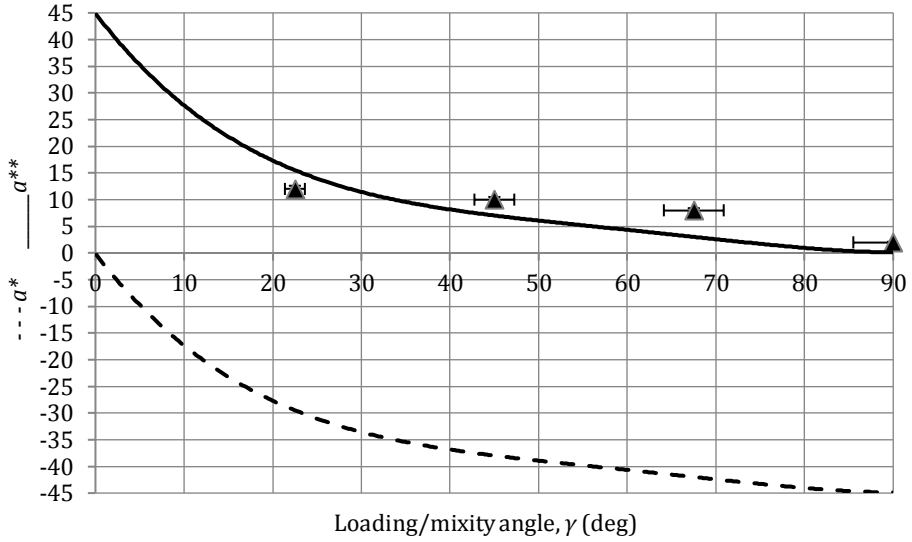

Fig. 13. α^* and α^{**} vs loading/mixity angle γ , ▲ experimental showing the standard error.

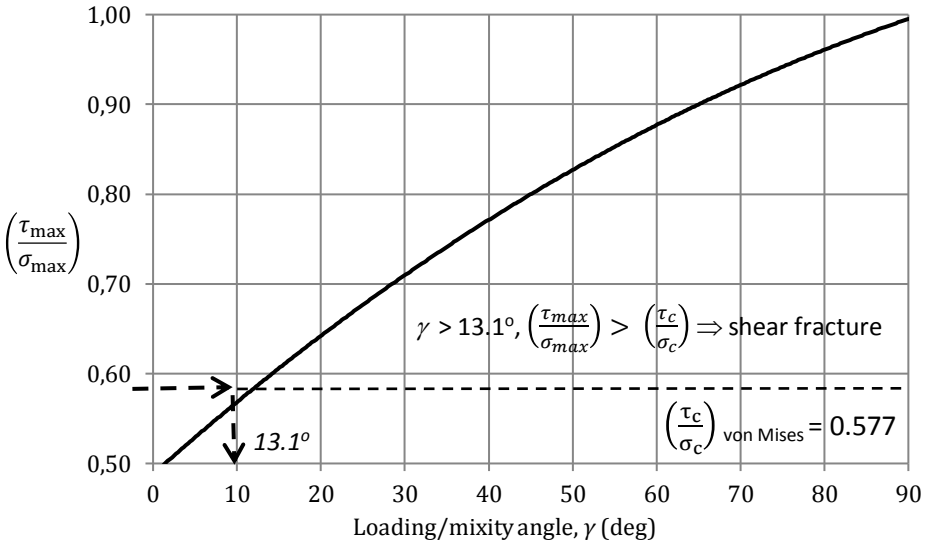

Fig. 14. $\tau_{\max}/\sigma_{\max}$ vs loading/mixity angle, γ.

For the test specimen, using this set-up of mode I/III fracture, for the experimental variation of γ, $22.5^0 < \gamma < 90^0$, theory predicts that failure is by shear. To check the validity of this statement for each mode mixity angle γ the average experimental α^{**} (for shear failure) are evaluated and compared with the experimentally measured angles as given in Table 6 (the values of α represent the average values of the varying leg widths and material thickness). The angles measured for both sheet thickness showed very similar results, the only slightly noticeable differences are that in some of the 1.0mm sheet, shear lips with a central slant were only slightly visible. The phenomena associated with ductile fracture surfaces when plane strain is characteristic of the interior material, where the adjacent material prevents lateral contraction and at the surface plane stress prevails.

Table 6. Crack plane slant angle, $\boldsymbol{\alpha}$ for the various loading mixity, $\boldsymbol{\gamma}$.

mode mixity γ (deg)	α exp (deg)	α^{**} theo (deg)	α^{*} theo (deg)
90 (mode III)	2	0.00	-45.00
67.5	8	2.95	-42.04
45	10	7.02	-37.98
22.5	12	15.56	-29.44
0 (mode I)	N/A	45.00	0.00

The results presented here have conclusively shown that Hill's theory is valid, the comparison and use of the work/energy approach with the crack tip stress approach can be combined and utilised and the fracture mechanism (tensile or shear) can be predicted together with the numerical values of the slant crack angle.

5. Conclusions

The investigation clearly shows a link between the application of the two well-known methods of crack tip stresses and the energy based equations governing crack initiation and propagation in the mixed mode I/III fields. The Maximum Hoop stress Criterion (MHSC) and the Maximum Normal Stress Criterion (MNSC), together with the Tresca and Von-Mises failure theories have successfully been applied to determine the fracture type when the specimens are subjected to a mode I/III field loading. The two leg trouser test specimen which is successful in pure mode III applications using the energy approach was further extended to determine the mixed mode I/III essential work of fracture by varying the mode mixity angle from 0^o (pure mode I) to 90^o (pure mode III). Together with Hill's criterion for ductile fracture the ratio of the essential work of fracture under both modes, consequentially the stress intensity factors and direction of relative motion was predicted according to the mode mixity angle. The energy approach using a locus of constant essential work of fracture for each mixity angle was found and the same expected trend of falling force per unit thickness as the leg width increased was shown. The total mode mixity essential work was successfully portioned to each % contribution to both modes, R_I and R_{III}, as the mixity angle was varied. The R_I/R_{III} and K_I/K_{III} using both the energy and the crack tip stress approaches showed good agreement. For the DX51D sheet material, $0.7 < \tau_c/\sigma_c < 0.8$ show that the crack tip stress theory predicts crack angles in good agreement with experiment. Using the Von-Mises failure criterion, the transition from tensile to shear fracture occurs when the mode mixity angle is small, 13.1^o and slant angle, i.e. the "rooftop" is 23.5^o with $K_I/K_{III} < 2.156$ for all results.

References

Anderson TL (2005). Fracture Mechanics*:* Fundamentals and Applications. 3rd ed., Taylor & Francis.

Atkins AG, Mai YW (1985). Elastic and Plastic Fracture: Metals, Polymers, Ceramics, Composites, Biological Materials. Ellis Horwood Limited.

BS EN ISO 6892-1 (2009). Metallic materials- Tensile testing. Part 1: Method of test at ambient temperature.

Chai H (1988). Shear fracture. *International Journal of Fracture*, 37, 137–159.

Chao YJ, Liu S (1997). On the failure of crack under mixed-mode loads. *International Journal of Fracture*, 87, 201–223.

Chao YJ, Zhu XK (1999). A simple theory for describing the transition between tensile and shear mechanisms in Mode I, II, III and mixed-mode fracture. *In Mixed-mode Crack Behaviour*, [ed.] McDowell D. L. Miller.

Chen X, Jiao G, Cui Z (1986). Application of combined-mode fracture criteria to surface crack problems. *Engineering Fracture Mechanics*, 24(1), 127–144.

De Marco Muscat-Fenech CM, Ciappara S (2013). Connecting the Essential Work of Fracture, Stress Intensity Factor, Hill's Criterion in Mixed Mode I/II Loading. *International Journal of Fracture*, 183, 187-202. DOI 10.1007/s10704-013-9886-4.

Eftis J, Liebowitz H (1972). On the modified Westergaard equations for certain plane crack problems. *International Journal of Fracture,* 8, 383.

Erdogan F, Sih GC (1963). On the crack extension in plates under plane loading and transverse shear. *ASME Journal of Basic Engineering*, 85D, 519–527.

Feng X, Kumar AM, Hirth JP (1993). Mixed mode I/III fracture toughness of 2034 aluminium alloys. *Acta Metallurgical Materials*, 41(9), 2755–2764.

Helm JD, Sutton MA, Boone ML (2001). Characterizing crack growth in thin aluminium panels under tension-torsion loading using three-dimensional digital image correlation. *American Society for Testing and Materials*, STP 1323, 3–14.

Helm JD, Sutton MA, Dawicke DS, Boone ML (1997). 3D computer vision applications for aircraft fuselage materials and structures. *1st joint DoD/FAA/NASA Conference on Aging Aircraft* in Ogden, Utah, 1327–1341.

Hill R (1953). A new method for determining the yield criterion and plastic potential of ductile metals. *Journal of the Mechanics and Physics of Solids*, 1, 271- 276.

Hsia KJ, Zhang TL, Socie DF (1995). Effect of crack surface morphology on the fracture behaviour under mixed mode loading. *Theoretical and Applied Mechanics Report*, No. 799, UILU-ENG-95-6021.

Hui CY, Zehinder AT (1993). A theory for the fracture of thin plates subjected to bending and twisting moments. *International Journal of Fracture*, 61, 211–229.

Irwin GR (1957). Analysis of stresses and strains near the end of a crack traversing a plate. *Journal of Applied Mechanics*, 24, 361–260.

K. L. West Conshohocken American Society for Testing and Materials (1999). ASTM STP 1359, Philadelphia, 41–57.

Karmat SV, Hirth JP (1994). A mixed mode fracture toughness correlation, *Scripta Metallurgica et Materialia*, 30, 145–148.

Karmat SV, Hirth JP (1996). Effect of aging on mixed-mode I/III fracture toughness of 2034 aluminium alloys. *Act Materialia*, 44 (3), 1047–1054.

Knauss W (1970). An observation of crack propagation in anti-plane shear. *International Journal of Fracture,* 6(2), 183–187.

Lan W, Deng X, Sutton MA, Cheng CS (2006). Study of slant fracture in ductile materials. *International Journal of Fracture*, 141, 469–496.

Li Y, Wierzbicki T, Sutton MA, Yan J, Deng X (2011). Mixed mode stable tearing of thin sheet Al 6061-T6 specimens: experimental measurements and finite element simulations using a modified Mohr-Coulomb fracture criterion. *International Journal of Fracture*, 168, 53–71.

Lui S, Chao YJ, Zhu X (2004). Tensile-shear Transition in mixed mode I/III fracture. *International Journal of Solids Structures,* 41, 6147–6172.

Macagno TM, Knott JF (1989). The fracture behaviour of PMMA in mixed modes I and II. *Engineering Fracture Mechanics*, 34, 65–86.

Macagno TM, Knott JF (1992). The mixed modes I/II fracture behaviour of lightly tempered HY130 steel at room temperature. *Engineering Fracture Mechanics*, 41, 805–820.

Mai YW, Cotterell B (1984). The Essential Work of Fracture of the Tearing of Ductile Sheet Materials. *International Journal of Fracture*, 24, 229–236.

Muscat-Fenech CM (1992). Tearing of Sheet Materials. Edition PhD. - Doctor of Philosphy in Engineering, Publisher Department of Engineering, University of Reading, U.K., BLDSC identification no.: DX 173965, University of Reading, reading, U.K.

Muscat-Fenech CM, Liu JH, Atkins AG (1992). The trousers tearing test with ductile metal sheets. *Journal of Materials Processing Technology*, 32(1–2), 301-315.

Muscat-Fenech CM, Atkins AG (1994a). Elastoplastic trouser tear testing of sheet materials. *International Journal of Fracture*, 67, 69–80.

Muscat-Fenech CM, Atkins AG (1994b). Elastoplastic convergent and divergent crack paths in tear testing of sheet materials. *Fatigue Fracture of Engineering Materials and Structures*, 17(2), 133–143.

Pan J, Shih CF (1992). Elastic – plastic analysis of combined I, II and III crack tip fields under small scale yielding conditions. *International Journal of Solids Structures,* 29 (22), 2795–2814.

Pook LP (1985). Comments on fatigue crack growth under mixed mode I and III and pure mode III loading. Multi-axial Fatigue. ASTM STP 853, in Miller, K.J., Brown, M.W., (Eds), *American Society for Testing and Materials*, Philadelphia, 259–263.

Pook LP, Sharples JK (1979). The mode III fracture crack growth threshold for mild steel, *International Journal of Fracture*, 15, R223–R226.

Rivlin RS, Thomas AG (1953). Rupture of rubber. I. Characteristic energy for tearing. *Journal of Polymer Science,* 10(3), 291–318

Royer J (1988). Study of pure mixed-mode fracture of a brittle material. *Experimental Mechanics*, 28, 382–387.

Sanford RJ (1979). A critical re-examination of the Westergaard method for solving opening mode crack problems. *Mechanics Research Communications*, 6, 289–294.

Shah RC (1974). Fracture under combined modes in 4340 steel. Fracture Analysis, *ASTM* STP 560, in*:* American society for testing and materials, 29–52.

Sih GC (1966). On Westergaard method of crack analysis. *International Journal of Fracture,* 2, 628 – 631.

Sih GC, Barthelemy BM (1980). Mixed mode fatigue crack growth predictions. *Engineering Fracture Mechanics*, 13, 439–451.

Sih GC, Cha BCK (1974). A fracture criterion for three-dimensional crack problems. *Engineering Fracture Mechanics*, 6, 699–723.

Sneddon N (1946). The distribution of stress in the neighbourhood of a crack in an elastic solid. *Proc. R. Soc. London. Ser. A* , A-187, 229–260.

Sommer E (1969). Formation of fracture 'lances' in glass. *Engineering Fracture Mechanics*, 1, 539–546.

Suresh S, Shih CF, Morrone A, O'Dowd NP (1990). Mixed-mode plane strain crack problems. *ASTM* STP 560, 187–210.

Suresh S, Tschegg EK (1987). Combined mode I – mode III fracture of fatigue – precracked alumina. *Journal of American Ceramic Society*, 70(10), 726–733.

Sutton MA, Helm JD, Boone ML (2001). Experimental study of crack growth in thin sheet 2024-T3 aluminium under tension-torsion loading. *International Journal of Fracture,* 109, 285–301.

Tian D, Lu D, Zhu J (1982). Crack propagation under combined stresses in three dimensional medium. *Engineering Fracture Mechanics*, 63, 5–17.

Wei Z, Deng X, Sutton MA, Yan JH, Cheng CS, Zavattieri P (2011). Modelling of mixed-mode crack growth in ductile thin sheets under combined in-plane and out-of plane loading. *Engineering Fracture Mechanics*, 78, 3082–3101.

Wei Z, Yan JH, Deng X, Sutton MA, Cheng CS (2005). Study of Mixed-Mode I/III Fracture in Ductile Materials. In Proceedings of the 2005 *SEM Annual conference and exposition on experimental and applied mechanics*, Portland, Oregon, June 7–9, 1651–1655.

Westergaard HM (1939). Bearing pressures and cracks. *Journal of Applied Mechanics,* 6, 49–53.

Williams JG, Ewing PD (1972). Fracture under complex stress–the angled crack problem. *International Journal of Fracture,* 8, 441–446.

Williams ML (1957). On the stress distribution at the base of a stationary crack. *Journal* of Applied *Mechanics,* 24, 109–114.

Yan JH, Sutton MA, Deng X, Cheng CS (2007). Mixed-mode fracture of ductile thin-sheet materials under combined in-plane and out-of-plane loading. *International Journal of Fracture,* 144, 297–321

Yan JH, Sutton MA, Deng X, Wei Z, Zavattieri P (2009). Mixed-mode crack growth in ductile thin sheet materials under combined in-plane and out-of-plane loading. *International Journal of Fracture,* 160, 169–188.

Yates JR, Miller KJ (1989). Mixed mode (I+III) fatigue thresholds in a forging steel. *Fatigue and Fracture Engineering Materials and Structures,* 12(3), 259–270.